Progress In Electromagnetics Research, Vol. 105, 141–155, 2010

AN ADAPTIVE CAVITY SETUP FOR ACCURATE MEASUREMENTS OF COMPLEX DIELECTRIC PERMITTIVITY

G. Addamo, G. Virone, D. Vaccaneo, R. Tascone, O. A. Peverini, and R. Orta

Istituto di Elettronica ed Ingegneria dell'Informazione e delle Telecomunicazioni (IEIIT-CNR)
Politecnico di Torino, I-10129 Turin, Italy

Abstract—In order to enhance the accuracy of the complex permittivity data employed in Ground Penetrating Radar (GPR) techniques, an adaptive cavity setup is presented. The use of moveable walls permits to relax the mechanical constraints on the sample dimensions so that it can be employed also in complicate measurement condition as, for example, in the case of wet samples. Moreover, exploiting the cavity resonance phenomenon, low loss materials, such as some type of marbles, can be accurately evaluated. The numerical characterization, the parametric analyses and the L-band measurement results show the validity and the reliability of this configuration.

1. INTRODUCTION

Among the geophysical methods employed at microwave frequencies, the ground penetrating radar (GPR) technique represents an interesting and cheap approach for a not invasive analysis of a variety of media including rock, soil, ice and water [1, 2]. Engineering applications of the GPR include non destructive testing of structures and pavements, locating buried structures and analyzing the preservation state of historical buildings. The analysis and processing of GPR data require an accurate estimation of the complex dielectric permittivity of the material under test (MUT) over a broad frequency range (typically GPR frequencies range from 0.5 GHz to 2.5 GHz). The use, for this purpose, of an open ended coaxial probe presents various advantages in terms of simplicity and flexibility of the measurement.

Corresponding author: G. Addamo (giuseppe.addamo@polito.it).

However, this system presents several drawbacks in the case of solid materials with low losses, such as some kind of marbles [3–10]. The measurement is indeed sensitive to the MUT surface roughness and the presence of local defects, such as voids or grains, has a strong influence on the measurement accuracy.

To enhance the accuracy of this setup in sub-bands of the GPR frequency span, in this work we propose a characterization obtained by measurements of the transmission coefficient S_{21} under resonance conditions [11, 12] and [13]. We will focus on the L-band, i.e., 1–2 GHz. However, a similar system can be employed in the other sub-bands. A first waveguide setup was described in a previous paper, where a cavity was constructed by means of two rectangular irises in a standard WR650 waveguide [14]. The MUT was placed in the cavity and was supposed to fill completely the cross section. This setup permits to obtain good levels of accuracy but is limited by very stringent requirements on the MUT dimensions. Although the standard sample manufacture procedure can indeed guarantee the required brick-shape, i.e., planar parallel surface, the usual tolerances on the dimensions are larger than 2 millimeters. The insertion and extraction of the samples are therefore quite problematic and require particular care and long time. This fact is a clear drawback when wet samples are analyzed. On the other hand, smaller samples produce air gaps which can lead to more complicate electromagnetic phenomena such as multiple peaks in the transmission coefficient curve. All these drawbacks have been overcome by means of a new measurement setup based on an adaptive cavity whose preliminary theoretical study was presented in [15]. The numerical characterization and the experimental validation of the setup and of the measurement technique are presented in the following section.

2. MEASUREMENT SETUP

2.1. Description

The main idea of this new setup is to employ a waveguide whose cross section fits that of the MUT. In this way, the constraints on the MUT dimensions are relaxed. This goal is obtained by means of a rectangular waveguide with two moveable walls (see Figure 1). One is the top wall which can be completely removed in order to place accurately the sample. The other is a sliding lateral wall, which runs along rails. The sample is inserted in the waveguide from the top and then is pressed by the sliding wall in order to fix its position (see Figures 2 and 3). In this way, the actual position of the MUT is well controlled and the coaxial cables of the network analyzer are not moved during the insertion of

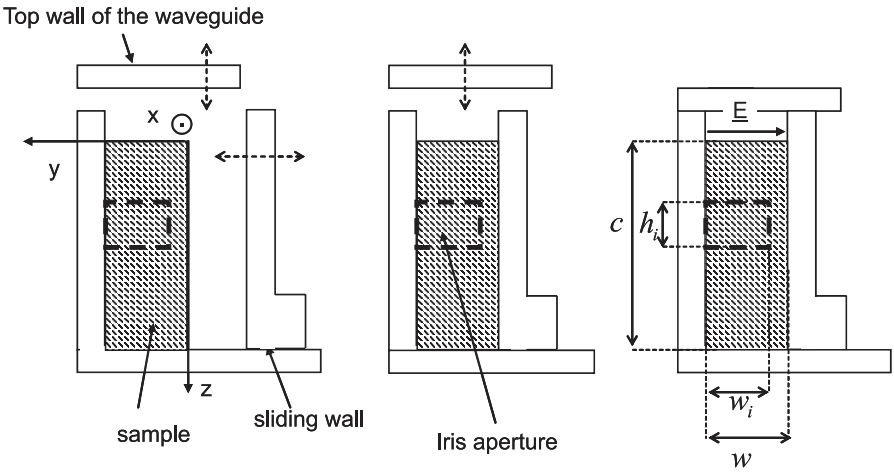

Figure 1. Schematic representation of the insertion and locking of the MUT in the cavity.

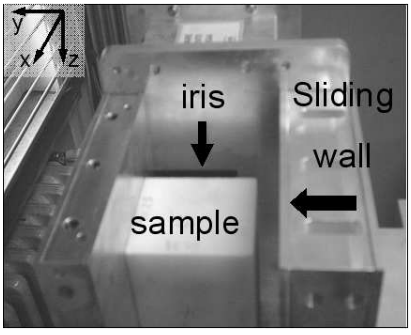

Figure 2. Picture of the open adaptive cavity with the sample inside. The top wall has been removed.

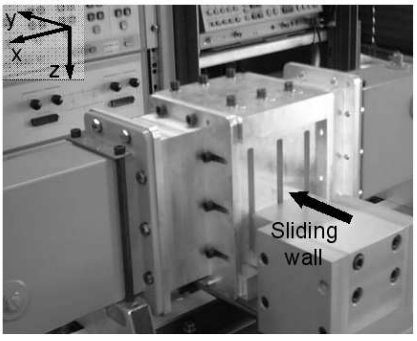

Figure 3. Picture of the closed measurement setup.

the samples to guarantee the stability of the calibrated setup. Note that the air gap along the broad waveguide wall (that is perpendicular to the electric field) is completely removed in this configuration. Even a small air gap in this direction has indeed a strong influence on the frequency response of the cavity. This statement is confirmed by the plots shown in Figure 4, where the S_{21} curve as a function of frequency is reported in the case of an air gap equal to zero and 2 mm. The effects of the gap parallel to the electric field, still present in this configuration,

are less significant and are discussed in the Section 3.

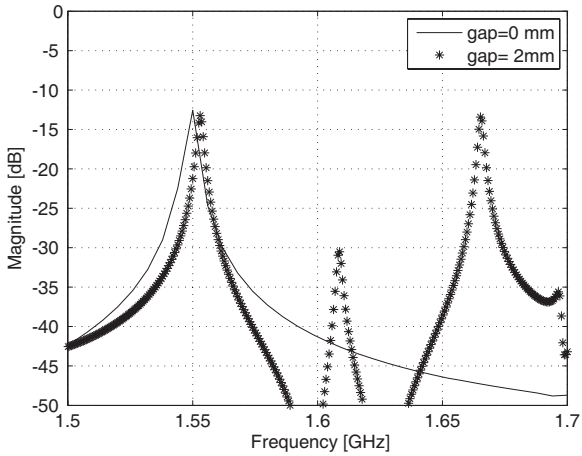

Figure 4. Influence on the transmission curve of an air gap perpendicular to the electric field. Note the appearance of multiple peaks with a gap of only 2 mm. The sample has $\epsilon_r = 8.5$, $\rho = 0.9\,\mathrm{k\Omega m}$ and length $L_s = 70\,\mathrm{mm}$.

The overall cavity is composed by this adaptive waveguide and two rectangular irises. Their position with respect the sample is shown in Figures 6. The setup has been designed for samples with width w in the range $[64, 93]$ mm and height c lower than 165.1 mm, i.e., the width of the WR650 waveguide. Note that the value of w fixes the narrow side of the rectangular waveguide. The cavity length is $L = 156\,\mathrm{mm}$ and the rectangular apertures of the 1 mm-thick irises ($w_i = 63\,\mathrm{mm}$, $h_i = 33.09\,\mathrm{mm}$) have been chosen so that the resonance frequency of the unloaded cavity is equal to 1.3 GHz.

2.2. Numerical Characterization of the Setup

The electromagnetic model of the setup can be constructed by means of the generalized scattering matrices (GSM) of the single blocks. The TE_{10} mode incident on the rectangular aperture of the 1 mm-thick irises ($h_i = 63.1\,\mathrm{mm}$, $w_i = 33.09\,\mathrm{mm}$) excites the modes $TE_{m,n}$ and $TM_{m,n}$ with odd m. Moreover, the partially filled waveguide (PFW) couples the modes of the rectangular waveguide, therefore a complete multimode description of the irises is necessary. The relevant GSM has been obtained by the coupled integral equation technique (CIET) [16]. The metal losses are introduced in the model by means of an equivalent metal resistivity equal to $0.1\,\mu\Omega\mathrm{m}$. This value has been determined

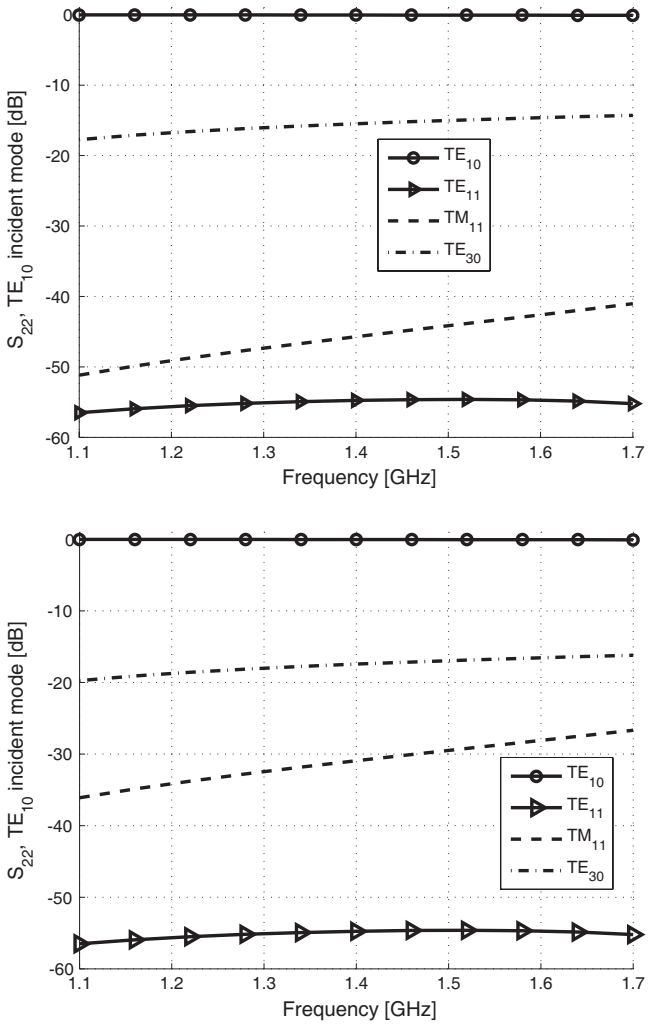

Figure 5. Magnitude of S_{22} direct and cross terms of the rectangular aperture iris for the case of $h_i = 63.1\,\text{mm}$ (top figure) and $h_i = 82.5\,\text{mm}$ (bottom figure).

experimentally by measuring the unloaded cavity and is much greater than the usual copper bulk resistivity (0.017 $\mu\Omega$m), since it takes into account also the roughness of the metallic surfaces. As an example, Figure 5 shows the magnitude, in dB, of the S_{22} matrix direct and cross terms for the first waveguide modes for the cases of $h_i = 63.1\,\text{mm}$ and

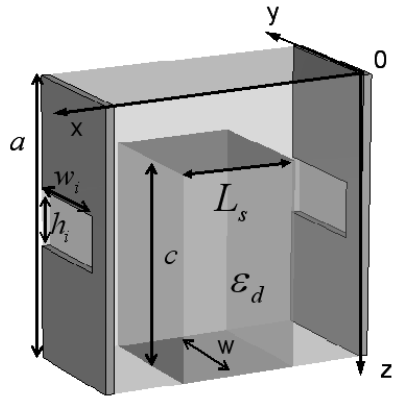

Figure 6. Sketch of the adaptive cavity. The analysis is carried out by looking at the z axis.

$h_i = 82.5\,\text{mm}$.

Under the assumption of homogenous, perfect brick and isotropic MUT, the waveguide cross section is filled only partially, leaving an air gap parallel to the electric field, as it can be observed in Figure 1. Let a and c be the broad side of the waveguide and the MUT height, respectively. The GSM of the cavity can be computed by means of the Mode-Matching technique, which requires the knowledge of the modal spectrum of the PFW [17, 18]. The modes of this structure can be computed by applying the resonance condition at the air-dielectric interface, but this procedure leads to a complex transcendental equation whose solution is not straightforward. Although complex function theory can be used to simplify this task [19, 20], we opted for a more automatic and rapidly convergent numerical technique which we describe in detail. With reference to the geometry of Figure 6, it can be shown that the z-dependance of the TE_z and TM_z mode functions of the loaded waveguide can be derived from the solution of the following boundary-value problem:

$$\begin{cases} \dfrac{d^2}{dz^2}V_{TE} + \left(k_0^2\epsilon_{e,d} - \left(\dfrac{n\pi}{w}\right)^2\right)V_{TE} = \beta_{TE}^2 V_{TE} \\ V(0) = V(a) = 0 \\ V(c^-) = V(c^+) \end{cases} \tag{1}$$

$$\begin{cases} \dfrac{d^2}{dz^2} I_{TM} + \left(k_0^2 \epsilon_{e,d} - \left(\dfrac{n\pi}{w} \right)^2 \right) I_{TM} = \beta_{TM}^2 V_{TM} \\ I(c^-) = I(c^+) \\ \dfrac{dI}{dz}(z=0) = \dfrac{dI}{dz}(z=a) = 0 \end{cases} \tag{2}$$

In (1) and (2), n is the modal index pertaining to the y direction, β is the modal propagation constant and $\epsilon_{e,d}$ are the dielectric permittivities of the air and the MUT, respectively. Moreover, V is proportional to E_y and I to H_y. As usual, the mode functions are determined by neglecting the limited wall conductivity, which is accounted for perturbatively in the propagation constant. In any case, the losses due to the dielectric are much higher than those due to the metallic walls. Let us consider in detail the TE case. The differential eigenvalue problem (1) is solved by a spectral method based on orthogonal polynomials, [21, 22]. The eigenfunctions $V_{e,d}(z)$ are C^∞ everywhere apart from the interface, where they are only C^1 (C^0 in the TM case). For this reason, if a single-domain method is applied, a very large number of polynomials is required in order to obtain a good approximation of the solution. However, it is well-known that exponential convergence rate of spectral methods can be reestablished by applying an appropriate domain decomposition. For the structure under analysis, it is sufficient to define two separate sets of Legendre polynomials in the air gap and in the dielectric region. If N_e and N_d are the number of polynomials used in the two subregions, the modal voltages are written as:

$$V_e(z) = \sum_{n=0}^{N_e} e_n P_n(\xi_e)$$

$$V_d(z) = \sum_{n=0}^{N_e} d_n P_n(\xi_e)$$

where $\xi_{e,d}(z)$ are linear functions which map the two domains $0 \le z \le c$ and $c \le z \le a$ onto $[-1, 1]$. The second derivative term in (1) can be written as:

$$\frac{d^2}{dz^2} V_e(z) = \frac{2}{c} \sum_{k=0}^{N_e-2} f_k P_k(\xi_e)$$

$$\frac{d^2}{dz^2} V_d(z) = \frac{2}{a-c} \sum_{k=0}^{N_d-2} g_k P_k(\xi_d)$$

where

$$f_k = \left(k + \frac{1}{2}\right) \sum_{m=k+2,k+4}^{N_e} (k+m+1)(m-k)e_m$$

$$g_k = \left(k + \frac{1}{2}\right) \sum_{m=k+2,k+4}^{N_d} (k+m+1)(m-k)d_m$$

By substituting the previous relations into (1) and by projecting onto the two sets of polynomials (Galerkin procedure) one obtains the following equivalent algebraic eigenvalue problem:

$$\underline{\underline{A}}\,\underline{x} = \beta^2 \underline{x} \tag{3}$$

where $\underline{x} = [e_0\, e_1 \ldots e_{N_e-2}\, d_0\, d_1 \ldots d_{N_d-2}]^T$. It has to be noted that the unknowns $[e_{N_e-1}\, e_{N_e}\, d_{N_d-1}\, d_{N_d}]$ can be computed as a linear combination of the $\underline{x}$ elements because of the boundary conditions. The code is very fast since the matrix elements are known analytically, of course. It has been numerically proved that the optimum ratio between the number N_e and N_d of polynomials, to be used in the two subregions, is

$$\frac{N_e}{N_d} \approx \frac{c}{(a-c)\sqrt{\epsilon_{rd}}} \tag{4}$$

As a rule of thumb, only half of the computed eigenvalues proved to be a good estimate of the desired propagation constants. Usually 40 polynomials guarantee a very accurate computation of the field in the PFW. At this stage of the numerical characterization of the setup, the scattering matrix of the dielectric block can be obtained by solving a junction-problem between the empty waveguide and the PFW.

2.3. Parametric Analysis

The simulation model has been used to analyze the effect of the air gap parallel to the E-field. Figure 7 shows the plots of the transmission coefficient versus the frequency for various values of the air gap. The sample data are: permittivity $\epsilon_r = 8.5$, resistivity $\rho = 0.9\,\mathrm{k\Omega m}$, width $w = 79.9\,\mathrm{mm}$ and length $L_s = 70.2\,\mathrm{mm}$. The height changes so that the air gap thickness varies between 0 and 35 mm. It can be noticed that the resonance frequency has a weak dependence on the air gap thickness for values lower than 40 mm. Nevertheless, its effect is taken into account in the parameters extraction procedure.

Figure 8 shows the iso-level curves of the resonance frequency and of the maximum transmission coefficient in the (ϵ_r, ρ) plane. The

curves refer to an air gap of 30 mm and a sample with $w = 82.55\,\text{mm}$ and length $L_s = 50\,\text{mm}$. The figure shows that the mapping Π: $(\epsilon_r, \rho) \mapsto (f_r, |S_{21}|_{\max})$ is invertible since the two families of curves are almost orthogonal. Moreover, as it could be expected, the resonance frequency depends essentially on the permittivity ϵ_r whereas the peak transmission $|S_{21}|_{\max}$ depends primarily on the resistivity ρ. This fact was discussed in [14] only for $c = a$. In the extraction procedure, the determination of the pair (ϵ_r, ρ) is carried out by a least square optimization technique based on the minimization of the difference between the measured $|S_{21}^{(m)}|$ and computed $|S_{21}^{(c)}|$ amplitude of the transmission coefficient. In particular, the objective function to be minimized is defined as

$$F(\epsilon_r, \rho) = \sum_{f \in B} ||S_{21}^{(c)}(f)| - |S_{21}^{(m)}(f)||^2 \tag{5}$$

where B is a set of frequency points in the measurement band. According to the previous discussion it can be shown that the objective function $F(\epsilon_r, \rho)$ does not have local minima, therefore this extraction procedure is fast and reliable.

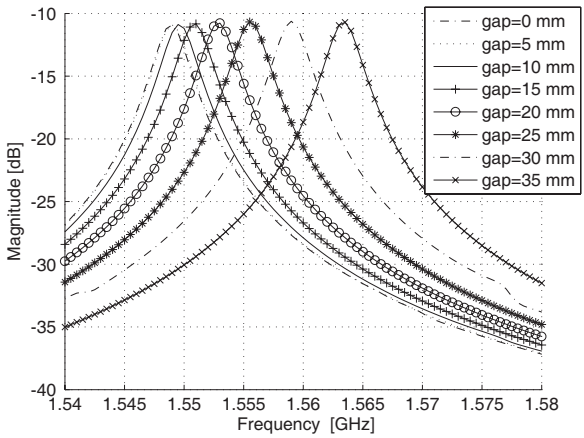

Figure 7. Computed transmission coefficient curves for various sizes of the air gap parallel to the electric field. The fixed sample dimensions are $w = 79.9\,\text{mm}$ and $L_s = 70.2\,\text{mm}$, while the permittivity is $\epsilon_r = 8.5$ and the resistivity $\rho = 0.9\,\text{k}\Omega\text{m}$.

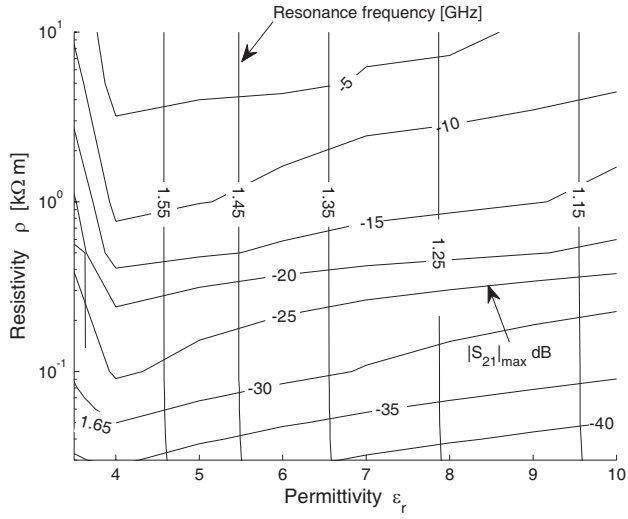

Figure 8. Iso-level curves of the resonance frequency and peak transmission coefficient as a function of the permittivity ϵ_r and resistivity ρ. An air gap of 30 mm is assumed. The MUT dimensions are $w = 82.5$ mm and $L_s = 50$ mm.

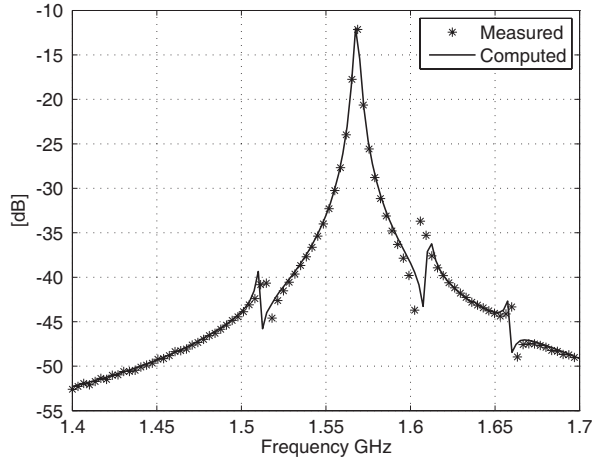

Figure 9. Comparison between measured and computed transmission coefficient for a Carrara marble sample of dimensions $w = 79.9$ mm, $c = 120.6$ mm and $L_s = 70.2$ mm.

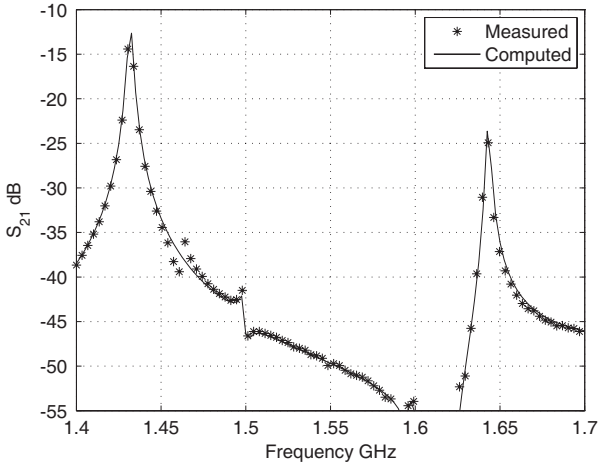

Figure 10. Comparison between measured and computed transmission coefficient for the same sample of Figure 9, rotated so that its dimensions are $w = 70.2\,\text{mm}$, $c = 120.6\,\text{mm}$ and $L_s = 79.9\,\text{mm}$.

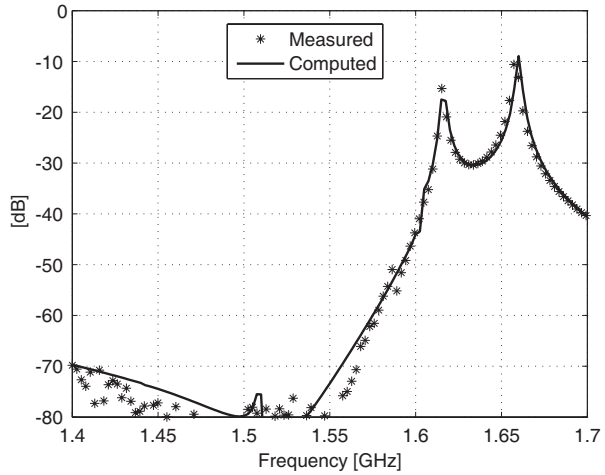

Figure 11. Comparison between measured and computed transmission coefficient for another Carrara marble sample whose dimensions are $w = 79.9\,\text{mm}$, $c = 70\,\text{mm}$ and $L_s = 73\,\text{mm}$.

3. MEASUREMENT RESULTS

Figure 9 shows a comparison between the measured and computed transmission coefficients for a Carrara marble sample. The dimensions are $w = 79.9\,\text{mm}$, $c = 120.6\,\text{mm}$ and $L_s = 70.2\,\text{mm}$. The computed curve has been obtained with estimated permittivity $\epsilon_r = 8.52$ and resistivity $\rho = 0.84$ kΩm. It is important to point out that a very good agreement has been achieved both close to the resonance and in the entire measurement band. It means that the complex permittivity of the MUT does not change significantly in the considered frequency band. In Figure 10, the same comparison is shown for the same sample but with a different orientation (90-deg rotation around the z axis, i.e., $w = 70.2\,\text{mm}$ and $L_s = 79.9\,\text{mm}$). In this case the extracted parameters are: $\epsilon_r = 8.45$ and $\rho = 0.91$ kΩm. The small differences can be related to the not perfect homogeneity of the sample. This assumption is confirmed by the data shown in Figure 11, which refer to another Carrara marble sample cut from the same block. The MUT dimensions are: $w = 79.9\,\text{mm}$, $c = 70\,\text{mm}$ and $L_s = 73.3\,\text{mm}$. In this case the extracted parameters are: $\epsilon_r = 8.50$ and $\rho = 0.91\,\text{k}\Omega\text{m}$. The presence of spurious peaks and the double resonances in the curves are related to the multimode propagation condition in the partially filled waveguide with the MUT. An extensive measurement campaign has shown the reliability and repeatability of the measurements and has permitted to estimate the uncertainty associated with the permittivity ϵ_r and resistivity ρ. The accuracy of these parameters is of the order of 1% for ϵ_r and 7% for ρ. The relevant measurements with an open ended coaxial probe show a dispersion of the order of 30% [23] and are quite sensitive to the pressure of the probe on the surface. Then the adaptive cavity setup presented in this work can be considered as a reliable reference.

4. CONCLUSIONS

A measurement setup based on an adaptive cavity has been presented. This setup has been designed to validate, in the L-band, the accuracy of broad band measurements of the dielectric properties of low loss rock material. The main advantage of the proposed configuration is that the waveguide walls can be moved to fit the sample dimension. In this way the problems related to the manufacture tolerances of the sample dimensions have been overcome. Similar setups can be built to cover other frequency bands. Future work will concern the generalization of the electromagnetic model for the measurements of anisotropic samples. The presented setup has been recently employed

for the electromagnetic characterization of other materials such as metallurgic powders and liquids. In this case, a suitable dielectric container has been employed and the relevant homogeneous dielectric layers have been considered in the electromagnetic model. Thanks to the flexibility of the adaptive cavity, the container dimensions can be properly designed in order to enhance the measurement sensitivity.

REFERENCES

1. Olhoeft, G. R., "Electromagnetic field and material properties in ground penetrating radar," *Advanced Ground Penetrating Radar*, 144–147, Proceedings of the 2nd International Workshop on May 14–16, 2003.
2. Soldovieri, F. and N. Romano, "The mutual interaction between the reconfigurable transmitting and receiving antennas in ground penetrating radar surveys," *Journal of Electromagnetic Waves and Applications*, Vol. 23, No. 14/15, 1919–1928, 2009.
3. Cardarelli, E., A. Godio, G. Morelli, L. Sambuelli, G. Santarato, and L. V. Socco, "Integrated geophysical surveys to investigate the Scarsella vault of St. John's baptistery in Florence," *The Leading Edge*, Vol. 21, No. 5, 467–470, 2002.
4. Mandeep, J. S., N. K. Loke, S. I. S. Hassan, M. F. Ain, S. Sreekantan, and K. Y. Cheong, "Investigation of microwave properties of high permittivity ceramic substrate," *Journal of Electromagnetic Waves and Applications*, Vol. 22, No. 14/15, 1873–1882, 2009.
5. Turner, G., A. F. Siggins, and L. D. Hunt, "Ground penetrating radar — Will it clear the haze at your site?" *Exploration geophysics*, Vol. 24, 819–832, 1993.
6. Wu, Y., Z. X. Tang, Y. Xu, X. He, and B. Zhang, "Permittivity measurement of ferroelectric thin film based on cpw transmission line," *Journal of Electromagnetic Waves and Applications*, Vol. 22, No. 4, 555–562, 2008.
7. Sambuelli, L., A. Godio, T. J. Guo, and L. V. Socco, "Laboratory determination of the dielectric permittivity of building stones in the 0.2–6 GHz band," *Proc. of the IV Meeting of the Environmental and Engineering Geophysical Society (European Section)*, 477–480, Barcelona, Spain, September 14–17, 1998.
8. Valagiannopoulos, C. A., "On measuring the permittivity tensor of an anisotropic material from the transmission coefficients," *Progress In Electromagnetics Research B*, Vol. 9, 105–116, 2008.
9. Bringhurst, S. and M. F. Iskander, "Thin sample dielectric

properties measurement using open-ended coaxial probes and FDTD calculations," *Antennas and Propagation Society*, Vol. 4, 1844–1847, June 1995.

10. Kumar, A. and G. Singh, "Measurement of dielectric constant and loss factor of the dielectric material at microwave frequencies," *Progress In Electromagnetics Research*, Vol. 69, 4754, 2007.
11. Rajab, K. Z., K. F. Fuh, R. Mittra, and M. Lanagan, "Dielectric property measurement using a resonant nonradiative dielectric waveguide structure," *IEEE Microwave and Wireless Components Letters*, Vol. 15, No. 2, 104–107, February 2005.
12. Akhtar, M. J., L. E. Feher, and M. Thumm, "A waveguide-based two-step approach for measuring complex permittivity tensor of uniaxial composite materials," *IEEE Transactions on Microwave Theory and Techniques*, Vol. 54, No. 5, 2011–2022, May 2006.
13. Atanaskovid, A., V. Tasi, and S. Ivkovid, "Automatization of the complex dielectric constant measurement," *Proc. of the 5th International Conference on Telecommunications in Modern Satellite, Cable and Broadcasting Service*, Vol. 2, 691–694, September 19–21, 2001.
14. Vaccaneo, D., L. Sambuelli, P. Marini, R. Tascone, and R. Orta, "Measurement system of complex permittivity of ornamental rocks in l frequency band," *IEEE Trans. on Geoscience and Remote Sensing*, Vol. 42, No. 11, 2490–2498, November 2004.
15. Vaccaneo, D., R. Tascone, and R. Orta, "Adaptive cavity for complex permittivity measurement of rock materials," *Proc. of the 2004 URSI EMTS*, Pisa, Italy, May 23–27, 2004.
16. Peverini, O. A., R. Tascone, M. Baralis, G. Virone, D. Trinchero, and R. Orta, "Reduced-order optimized mode-matching CAD of microwave waveguide components," *IEEE Trans. Microwave Theory Tech.*, Vol. 52, No. 1, 311–318, January 2004.
17. Itoh, T., *Numerical Techniques For Microwave and Millimeter-wave Passive Structures,* John Wiley & Sons Ltd., 1989.
18. Motavali, H. and A. Rostami, "Exactly modal analysis of inhomogeneous slab waveguide using nikiforov-uvarov method," *Journal of Electromagnetic Waves and Applications*, Vol. 22, No. 5/6, 681–692, 2008.
19. Lancellotti, V. and R. Orta, "Guided waves in layered cubic media: Convergence study of a polynomial expansion approach," *J. Acoust. Soc. Am.*, Vol. 104, No. 5, 2638–2644, November 1998.
20. Essid, C., M. B. B. Salah, K. Kochlef, A. Samet, and A. B. Kouki, "Spatial-spectral formulation of method of moment for rigorous

analysis of microstrip structures," *Progress In Electromagnetics Research Letters*, Vol. 6, 17–26, 2009.

21. Lin, H., G. Wang, and F. Liang, "A novel unconditionally stable pstd method based on weighted laguerre polynomial expansion," *Journal of Electromagnetic Waves and Applications*, Vol. 23, No. 8/9, 1011–1020, 2009.
22. Torre, A., "The relativistic hermite polynomials and the wave equation," *Progress In Electromagnetics Research B*, Vol. 16, 21–56, 2009.
23. Chen, C. P., M. Y. Chen, J. P. Yu, M. Niu, and D. Xu, "Uncertainty analysis for the simultaneous measurement of complex electromagnetic parameters using an open-ended coaxial probe," *Instrumentation and Measurement Technology Conference*, Vol. 1, 61–65, 2004.